

**Bubble Bursting: Universal Cavity and Jet Profiles**Ching-Yao Lai,<sup>1</sup> Jens Eggers,<sup>2</sup> and Luc Deike<sup>1,3,\*</sup><sup>1</sup>*Department of Mechanical and Aerospace Engineering, Princeton University, Princeton, New Jersey 08544, USA*<sup>2</sup>*School of Mathematics, University of Bristol, University Walk, Bristol BS8 1 TW, UK*<sup>3</sup>*Princeton Environmental Institute, Princeton University, Princeton, New Jersey 08544, USA* (Received 20 July 2018; published 2 October 2018)

After a bubble bursts at a liquid surface, the collapse of the cavity generates capillary waves, which focus on the axis of symmetry to produce a jet. The cavity and jet dynamics are primarily controlled by a nondimensional number that compares capillary inertia and viscous forces, i.e., the Laplace number  $La = \rho\gamma R_0/\mu^2$ , where  $\rho$ ,  $\mu$ ,  $\gamma$ , and  $R_0$  are the liquid density, viscosity, interfacial tension, and the initial bubble radius, respectively. In this Letter, we show that the time-dependent profiles of cavity collapse ( $t < t_0$ ) and jet formation ( $t > t_0$ ) both obey a  $|t - t_0|^{2/3}$  inviscid scaling, which results from a balance between surface tension and inertia forces. Moreover, we present a scaling law, valid above a critical Laplace number, which reconciles the time-dependent scaling with the recent scaling theory that links the Laplace number to the final jet velocity and ejected droplet size. This leads to a self-similar formula which describes the history of the jetting process, from cavity collapse to droplet formation.

DOI: [10.1103/PhysRevLett.121.144501](https://doi.org/10.1103/PhysRevLett.121.144501)

Bubbles bursting is ubiquitous in everyday life and is important for the climate, owing to the exchange of gas, water, heat, and chemical species between ocean and atmosphere [1–7]. After a bubble bursts, a jet forms and liquid drops detached from the jet are emitted to the atmosphere. The aerosol of drops (size ranges from 1 to 100  $\mu\text{m}$ ), which stays in the atmosphere is crucial since it regulates atmospheric chemistry [8], threatens human health by sending marine biotoxins and viruses to the atmosphere [9–11] and affects Earth’s radiation balance, cloud and ice crystals formation, and precipitation [7,12–15]. Due to the broad impact across a range of research fields, the dynamics of bubble bursting has been an active area of research for the past 60 years.

Much recent progress was made linking jet dynamics with the physical properties of the liquid. Ghabache *et al.* [16,17] developed scaling laws for the jet velocity as a function of the size of the jet drop, the liquid properties and the initial size of the mother bubble. A set of scaling laws for the jet velocity, as well as the radial and axial length of the jet as a function of the liquid properties, have been developed using a force and energy argument [18]. The effects of gravity were investigated theoretically [19]. The effect of gravity on jet velocity and the critical conditions for ejection of jet drops were examined numerically by Deike *et al.* [20].

Zeff *et al.* [21] showed that a liquid-water interface, before a surface wave collapses at time  $t_0$ , is self-similar and obeys a  $(t_0 - t)^{2/3}$  inertial-capillary scaling law, which has been shown to apply to cavity collapse [16,22] and jet formation near a critical Laplace number [23]. However, the existing  $(t_0 - t)^{2/3}$  scaling laws only describe the bursting

dynamics for a given set of fluid properties. The connection between the time-dependent self-similar scaling and a global scaling that involves fluid properties (e.g., the Ganan-Calvo scaling [18]) has not been addressed. Here, we present a universal scaling law for the dynamics of both cavity collapse ( $t < t_0$ ) and jet formation ( $t > t_0$ ), which incorporates both the time-dependent  $2/3$  scaling law and the Ganan-Calvo scaling [18] to describe the liquid-gas interface as a function of time  $t$ , liquid properties (viscosity  $\mu$ , interfacial tension  $\gamma$ , and density  $\rho$ ), and the initial bubble radius  $R_0$ .

We simulate numerically the dynamics of bubbles bursting using the open source solver Gerris with an adaptive mesh [24,25], which has yielded excellent agreement with experimental results [20,23]. We assume an axisymmetric system and solve the full two-phase Navier-Stokes equation. The relevant dimensionless numbers are the Bond number [ $Bo \equiv \rho g R_0^2/\gamma$  (relative importance of gravitational forces compared to surface tension forces)] and the Laplace number ( $La \equiv \rho\gamma R_0/\mu^2 = 1/Oh^2$  [20] [relative importance of surface tension forces to viscous forces]), where  $Oh$  is the Ohnesorge number. The initial static bubble shape depends only on  $Bo$ , and is computed by solving the Young-Laplace equations [26]. The time evolution of the liquid-gas interface  $h(r, t)$  for  $La = 2000$  and  $Bo = 10^{-3}$ , solved with a grid size up to  $4096^2$  and 819 grid points across the bubble diameter, is plotted in Fig. 1(a).

After a bubble bursts, capillary waves travel along the interface towards the bottom of the bubble cavity. A jet is formed when the capillary waves collapse and the curvature of the interface reverses at a time  $t_0$ . For  $La \geq La^* \approx 500$  [20,27], a jet drop detaches from the top of the jet at  $t_d$  after

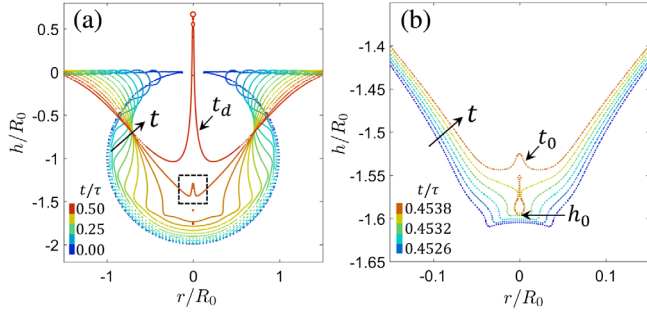


FIG. 1. The time evolution of the liquid-gas interface of a bursting bubble of initial radius  $R_0$  at  $La = 2000$  and  $Bo = 10^{-3}$ . The color bar indicates the time corresponding to different profiles. (a) The formation of a jet after the collapse of capillary waves. The time difference between the curves is  $\delta t/\tau = 0.038$ , where  $\tau = \sqrt{\rho R_0^3/\gamma}$  is the inertio-capillary timescale. The time when a jet ejects a drop is  $t_d$ . (b) The interface profiles right before a bubble is entrained. The time difference between the curves is  $\delta t/\tau = 0.0003$ . As the front of the capillary wave approaches  $r = 0$  the interface steepens, snaps, entrains a bubble, and forms a jet at  $t = t_0$ . The bottom location of the bubble at the entrapment is denoted with  $h_0$ .

the jet grows to a certain length. For  $La < La^*$  no drops detach from the liquid jet. The cavity profiles near the curvature reversal [dashed window in Fig. 1(a)] right before the jet forms at  $t_0$  is plotted in Fig. 1(b). The time difference between the curves is  $\delta t/\tau = 0.0003$ , where  $\tau \equiv \sqrt{\rho R_0^3/\gamma}$  is the inertio-capillary timescale. As time approaches  $t_0$ , the interface steepens and snaps, entrains a bubble and forms a jet at  $t_0$ . The lowest position of the profile at  $t_0$  is located at  $h = h_0$  and  $r = 0$ . In this Letter, we focus on the cases where  $Bo = 10^{-3}$  (which corresponds to a bubble of radius  $85 \mu\text{m}$  in water) so that the effects from gravity are negligible. Note that the jet velocity for  $Bo = 10^{-3}$  and  $10^{-2}$  are the same [20] and converge to the asymptotic limit where  $Bo = 0$ .

Assuming that during the curvature reversal the inertial forces are of the same orders of magnitude as the surface tension forces and the viscous forces, and that the initial surface energy of the bubbles supplies the viscous dissipation in the capillary waves and the kinetic energy in the jet formation, Ganan-Calvo obtained relationships involving the dimensionless parameter  $\varphi \equiv \sqrt{La}(\sqrt{La/La^*} - 1)$  [18]. For a jet near curvature reversal with a typical vertical speed  $V$ , radial speed  $V'$ , radial length scale  $R$ , and vertical length scale  $L$ ,

$$V/V_\mu = k_v \varphi^{-3/4}, \quad (1)$$

$$V'/V_\mu = k_{v'} \varphi^{-1/2}, \quad (2)$$

$$R/\ell_\mu = k_d \varphi^{5/4}, \quad (3)$$

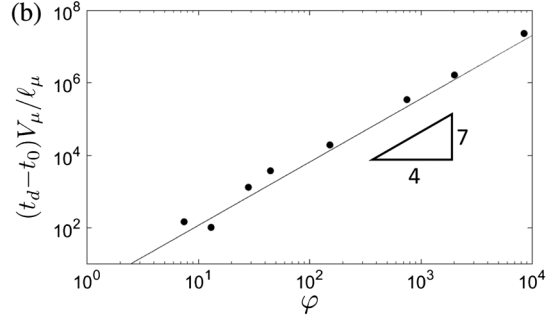
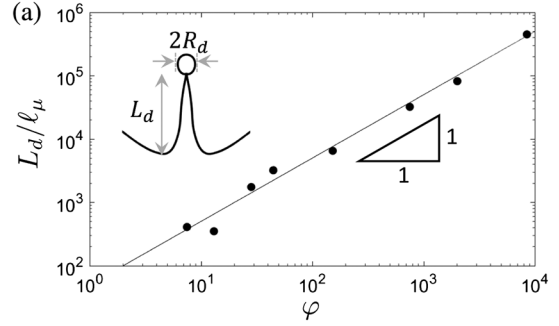


FIG. 2. Comparison between the numerical result (dots) and the scaling arguments (solid line) in Eqs. (4) and (5). When the jet drop detaches from the jet at  $t = t_d$ , the length of the jet and the radius of the jet drop are denoted  $L_d$  and  $R_d$ , respectively. (a) The numerical results show that the jet length  $L_d \propto \varphi$  obeys Eq. (4) with a fitted prefactor  $k_\ell \approx 50$  (solid line). (b) The timescale  $t_d - t_0$ , during which the jet forms and produces a jet drop, agrees well with the solid line  $(t_d - t_0) \propto \varphi^{7/4}$  [Eq. (5) with fitted prefactor  $k_t \approx 2$ ].

$$L/\ell_\mu = k_\ell \varphi, \quad (4)$$

where  $V_\mu \equiv \gamma/\mu$  and  $\ell_\mu \equiv \mu^2/\rho\gamma$ . For different  $La$  and  $Bo = 10^{-3}$ , we obtain numerically the drop radius  $R_d$ , the length of the jet  $L_d$  [defined in Fig. 2(a)] and the velocity of the drop  $V_d$  when a jet drop detaches at  $t_d$ . The numerical and experimental results of drop velocity  $V_d$  and radius  $R_d$  have been shown to agree well with Eqs. (1) and (3), respectively, with fitted prefactors  $k_v \approx 16$  and  $k_d \approx 0.6$  [18,20]. For Eq. (4), we choose the length of the jet  $L_d$  at  $t_d$  to be the axial length scale  $L$  and obtain good agreement between the numerical result and the scaling law with a numerical prefactor  $k_\ell \approx 50$ , as shown in Fig. 2(a) by the solid line.

A typical timescale for jet formation can be quantified using the time difference between the jet formation  $t_0$  and drop ejection  $t_d$ , i.e.,  $t_d - t_0$ . A natural timescale for the flow in the axial direction, using Eqs. (1) and (4), is  $L/V \sim \varphi^{7/4}$ . Therefore, we obtain a scaling relation for the axial timescale  $t_d - t_0$ ,

$$\frac{(t_d - t_0)}{\ell_\mu/V_\mu} = k_t \varphi^{7/4}, \quad (5)$$

which is in excellent agreement with our numerical results. Eq. (5) fitted to the numerical results ( $k_r \approx 2$ ) is shown by the solid line in Fig. 2(b). This discussion confirms the robustness of Ganan-Calvo's scaling law [18] to characterize the jet variables at drop detachment.

Now, we include the time-dependent dynamics in the scaling arguments [Eqs. (1)–(5)]. The free surface of the liquid-air interface [ $z = h(r, t)$ ] prior to cavity collapse ( $t = t_0$ ), assuming the flows are incompressible and irrotational, has been shown numerically and experimentally to be self-similar,

$$h(r, t) = (t_0 - t)^{2/3} f(r(t_0 - t)^{-2/3}), \quad (6)$$

where  $f$  is a function of the shape of the surface profile. Below we show that Eq. (6) not only applies to cavity collapse but also to the formation of the liquid jet for a wide range of La.

First, we combine the time-dependent scaling [Eq. (6)] with Eqs. (4) and (5), which includes the dependence of jet profiles  $h(r, t)$  on liquid properties ( $\mu, \gamma, \rho$ ). In Fig. 2 we show that the axial length scale  $L$  of the jet scales like  $\ell_\mu \varphi$  and the axial timescale of the jet ( $t_d - t_0$ )  $\approx \varphi^{7/4} \ell_\mu / V_\mu$ . Therefore, length and time in Eq. (6) can be rescaled using the characteristic length scale  $\ell_\mu \varphi$  and timescale  $t_j \equiv \varphi^{7/4} \ell_\mu / V_\mu$ , respectively. Therefore the dimensionless interface profiles during jet formation ( $t > t_0$ ) can be written as

$$\frac{h - h_b}{\ell_\mu \varphi} = \left( \frac{t - t_0}{t_j} \right)^{2/3} g_a \left[ \frac{r}{\ell_\mu \varphi} \left( \frac{t - t_0}{t_j} \right)^{-2/3} \right], \quad (7)$$

in which  $g_a$  is the dimensionless shape of the profile after the curvature reversal and  $h_b$  is the bottom location of the jet. To test Eq. (7) we plot the jet profiles for a range of Laplace number (La = 1000–50 000) at times  $t - t_0 = t_j, 3/2t_j, 2t_j, 5/2t_j$  in Fig. 3(a). After nondimensionalizing Fig. 3(a) using Eq. (7), the dimensionless jet profiles for different parameters La and different times collapse except for a region near the rounded tip, as shown by Fig. 3(b). Very close to the curvature reversal time during ( $t - t_0$ )  $< t_j$  the profiles fail to collapse, since the jet is comprised mostly by its rounded tip. We note that the size of the rounded tip of the jet does not vary much with time and is roughly the same size as the jet drop  $R_d$ , and thus scales as  $R \approx \ell_\mu \varphi^{5/4}$  [Eq. (3)]. While the size of the rounded tip and the jet drop are set by the radial length scale  $R$  at  $t = t_0$ , at long times, the radius of the jet body scales the same way as the axial jet length  $L \approx \ell_\mu \varphi$ , as predicted by Eq. (6).

On the other hand, before the cavity collapses ( $t < t_0$ ), capillary waves travel in the radial direction with a characteristic velocity  $V'$  [Eq. (2)]. The timescale for the capillary wave to reach the center, according to Eqs. (2) and (4), can be estimated as  $L/V' \approx \varphi^{3/2} \ell_\mu / V_\mu$ . Therefore we

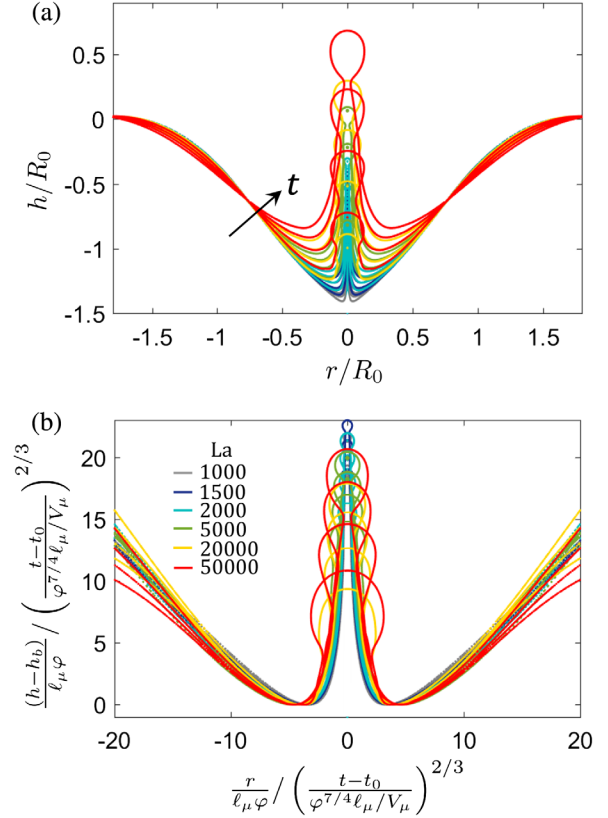


FIG. 3. (a) The time evolution of the liquid-gas interface during jet formation ( $t > t_0$ ) for La = 1000, 1500, 2000, 5000, 20 000, 50 000 at times  $t - t_0 = t_j, 3/2t_j, 2t_j, 5/2t_j$ , where  $t_j \equiv \varphi^{7/4} \ell_\mu / V_\mu$  is the characteristic time of jet formation. (b) The dimensionless jet profiles rescaled using Eq. (7). The profiles are shifted in the axial direction with respect to the bottom of the jet  $h_b$ . The dimensionless profiles for different times and La = 5000–50 000 collapse, except for the region of the rounded tip. When La  $\leq 2000$  (i.e.,  $\varphi \leq 45$ ) the timescale  $t_j$  used here deviates slightly from the jet lifetime  $t_d - t_0$  [see Fig. 2(b)], and therefore affects the collapse of the jet onto the universal profile.

define a characteristic time for the traveling capillary wave as  $t_c \equiv \varphi^{3/2} \ell_\mu / V_\mu$ . The cavity profiles at La = 1000–20 000 and  $t_0 - t = 6t_c, 8t_c, 10t_c$  are plotted in Fig. 4(b). For La = 1000–2000 only one capillary wave travels on the free surface, while for La  $\geq 5000$  multiple capillary waves are observed. Since the length scale of the capillary wave near the curvature reversal is set by the Ganan-Calvo length scale  $L \approx \ell_\mu \varphi$  [Eq. (4)], we nondimensionalize the  $(t_0 - t)^{2/3}$  self-similar cavity profiles [Eq. (6)] with the characteristic length scale  $\ell_\mu \varphi$  and radial timescale  $t_c$  of the capillary waves.

We propose that the dimensionless cavity profiles ( $t < t_0$ ) right before the capillary waves collapse obey

$$\frac{h - h_0}{\ell_\mu \varphi} = \left( \frac{t_0 - t}{t_c} \right)^{2/3} g_b \left[ \frac{r}{\ell_\mu \varphi} \left( \frac{t_0 - t}{t_c} \right)^{-2/3} \right], \quad (8)$$

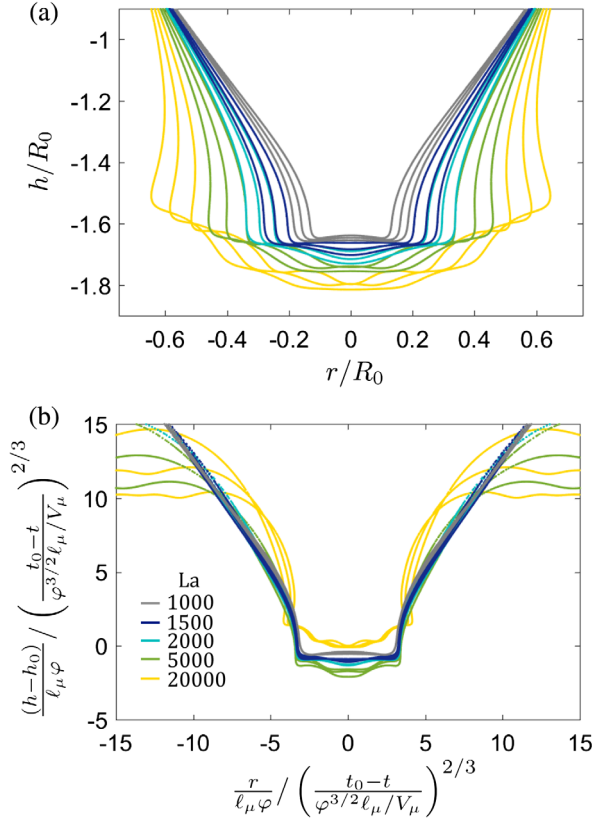


FIG. 4. (a) The time evolution of the interface during cavity collapse ( $t < t_0$ ) for  $\text{La} = 1000, 1500, 2000, 5000, 20000$  at times  $t_0 - t = 6t_c, 8t_c, 10t_c$ , where  $t_c \equiv \varphi^{3/2} \ell_\mu / V_\mu$  is the characteristic time of the horizontal capillary wave. (b) The rescaled cavity profiles nondimensionalized according to Eq. (8). The bottom of the bubble when bubble entrapment occurs ( $t = t_0$ ) is denoted  $h_0$ . The dimensionless profiles collapse onto a universal curve for  $\text{La} = 1000\text{--}5000$  during the time window  $t_0 - t = 6t_c - 10t_c$ . Near the bubble entrapment time  $t_0 - t < 6t_c$  the profile steepens and snaps, and thus deviates from the universal shape. When  $\text{La} \geq 5000$ , multiple capillary waves are observed [see (a)], and Eq. (8) does not collapse the profiles for  $\text{La} > 5000$ .

where  $g_b$  is the dimensionless shape of the profile before the curvature reversal and  $h_0$  [defined in Fig. 2(a)] is the location of the bottom of the bubble, also the location at which the capillary wave approaches at  $t_0$ . The cavity profiles in Fig. 4(a) rescaled using the universal self-similar scaling [Eq. (8)] collapse for different  $\text{La}$  and a period of time ( $6t_c \leq t_0 - t \leq 10t_c$ ) near  $t = t_0$ , as shown in Fig. 4(b). At  $\text{La} \geq 20000$ , multiple capillary waves appear and Eq. (8) fails to collapse the profiles. During  $t_0 - t < 6t_c$  the time is too close to the moment of curvature reversal, and the profiles deviate from the universal shape due to bubble pinch-off.

The differences between the dimensionless profiles for cavity collapse [Eq. (8), where  $t < t_0$ ] and jet formation [Eq. (7), where  $t > t_0$ ] are the choice of the timescale. Therefore, we can rewrite both dimensionless profiles, Eqs. (8) and (7), as

$$\mathcal{H}(\mathcal{R}, \mathcal{T}) = \mathcal{T}^{2/3} g_{a,b}(\mathcal{R}\mathcal{T}^{-2/3}) \quad (9)$$

where  $\mathcal{R} \equiv r/(\ell_\mu \varphi)$  is the dimensionless width. For cavity collapse the dimensionless length and time are  $\mathcal{H} \equiv [h(r, t) - h_0]/(\ell_\mu \varphi)$  and  $\mathcal{T} \equiv (t_0 - t)/t_c$ , respectively, where  $t_c \equiv \ell_\mu \varphi^{3/2}/V_\mu$  is the timescale of the traveling capillary wave. For jet formation,  $\mathcal{H} \equiv [h(r, t) - h_b]/(\ell_\mu \varphi)$  and  $\mathcal{T} \equiv (t - t_0)/t_j$ , where  $t_j \equiv \ell_\mu \varphi^{7/4}/V_\mu$  is the timescale of jet formation. The parameters that were found numerically are the bottom position  $h_b(t)$  of the jet, the bottom position  $h_0$  of the bubble, the time  $t_0$  when the curvature reverses, and the critical  $\text{La}$  for ejection of jet drops  $\text{La}^*$ . Eq. (9) agrees well with the dynamics of both cavity collapse (Fig. 3) and jet formation (Fig. 4) and connects the dynamics with time  $t$ , liquid properties ( $\mu, \gamma, \rho$ ), and initial bubble radius  $R_0$ .

The dynamics of the free surface away from the bubble entrapment time  $t_0$  obeys the  $|t - t_0|^{2/3}$  scaling for inviscid, incompressible, and irrotational flows. In our numerical simulation, we estimate the forces in the Navier-Stokes equation and find that at times, far away from  $t_0$ , the viscous forces are small compared with the inertia and surface tension forces. At  $t_0$  the viscous forces reach the same order of magnitude as the inertia and surface tension forces, in regions near high interface curvature. The effects of viscosity come into play during the curvature reversal at  $t_0$ , which set the length and velocity scales [Eqs. (1)–(4)] of the flows. Therefore, Eq. (9) successfully collapses the interface profiles for both  $t < t_0$  and  $t > t_0$  at different times and across a range of  $\text{La}$ .

In conclusion, we study the self-similar dynamics of a bursting bubble. We report the power-law dependence of the jet length and the timescale of the jet formation on the dimensionless parameter  $\varphi$ . The jet length  $L_d$  at the moment when a jet drop detaches is proportional to  $\varphi$ , agreeing well with Ganan-Calvo's scaling. The time from jet formation to drop detachment obeys  $t_d - t_0 \propto \varphi^{7/4}$ . Using proper length and timescales, we propose a scaling law to describe the dynamics of both cavity collapse and jet formation as a function of time, liquid properties, and the initial bubble size. We show that for a certain range of time and Laplace number, the dimensionless interfacial profiles collapse, exhibiting self-similar dynamics and good agreement with the universal scaling law.

We thank Howard A. Stone, Thomas Seon, and Stephane Popinet for helpful discussions. C. Y. L. acknowledges Andlinger Center for Energy and the Environment at Princeton University for partial support through the Maeder Graduate Fellowship. L. D. acknowledges support from the Princeton Environmental Institute at Princeton University and the Urban Grand Challenge program, and the Cooperative Institute for Climate Sciences between NOAA and Princeton University. J. E. acknowledges support by the Leverhulme Trust through International

Academic Fellowship IAF-2017-010. Computations were partially performed using allocation TG-OCE140023 to L. D. from the Extreme Science and Engineering Discovery Environment (XSEDE), which is supported by NSF Grant No. ACI-1053575.

---

\*ldeike@princeton.edu

- [1] J. Eggers and E. Villermaux, *Rep. Prog. Phys.* **71**, 036601 (2008).
- [2] C. F. Kientzler, A. B. Arons, D. C. Blanchard, and A. H. Woodcock, *Tellus* **6**, 1 (1954).
- [3] J. Wu, *J. Geophys. Res.* **78**, 511 (1973).
- [4] D. E. Spiel, *J. Geophys. Res.* **99**, 10289 (1994).
- [5] D. E. Spiel, *Tellus B* **46**, 325 (1994).
- [6] D. C. Blanchard, *J. Geophys. Res.* **94**, 10999 (1989).
- [7] F. Veron, *Annu. Rev. Fluid Mech.* **47**, 507 (2015).
- [8] X. Wang, G. B. Deane, K. A. Moore, O. S. Ryder, M. D. Stokes, C. M. Beall, D. B. Collins, M. V. Santander, S. M. Burrows, C. M. Sultana *et al.*, *Proc. Natl. Acad. Sci. U.S.A.* **114**, 6978 (2017).
- [9] R. H. Pierce, M. S. Henry, P. C. Blum, S. L. Hamel, B. Kirkpatrick, Y. S. Cheng, Y. Zhou, C. M. Irvin, J. Naar, A. Weidner *et al.*, *Harmful algae* **4**, 965 (2005).
- [10] E. R. Baylor, V. Peters, and M. B. Baylor, *Science* **197**, 763 (1977).
- [11] E. R. Baylor, M. B. Baylor, D. C. Blanchard, L. D. Syzdek, and C. Appel, *Science* **198**, 575 (1977).
- [12] B. Stevens and G. Feingold, *Nature (London)* **461**, 607 (2009).
- [13] G. Feingold, A. McComiskey, T. Yamaguchi, J. S. Johnson, K. S. Carslaw, and K. S. Schmidt, *Proc. Natl. Acad. Sci. U.S.A.* **113**, 5812 (2016).
- [14] O. Boucher, D. Randall, P. Artaxo, C. Bretherton, G. Feingold, P. Forster, V.-M. Kerminen, Y. Kondo, H. Liao, U. Lohmann *et al.*, in *Climate change 2013: the physical science basis. Contribution of Working Group I to the 5th Assessment Report of the IPCC* (Cambridge University Press, Cambridge, England, 2013), pp. 571–657.
- [15] R. J. Charlson, S. E. Schwartz, J. M. Hales, R. D. Cess, J. J. Coakley, J. E. Hansen, and D. J. Hofmann, *Science* **255**, 423 (1992).
- [16] E. Ghabache, A. Antkowiak, C. Josserand, and T. Séon, *Phys. Fluids* **26**, 121701 (2014).
- [17] E. Ghabache and T. Séon, *Phys. Rev. Fluids* **1**, 051901 (2016).
- [18] A. M. Gañán-Calvo, *Phys. Rev. Lett.* **119**, 204502 (2017).
- [19] A. M. Ganán-Calvo, arXiv:1806.04199 (to be published).
- [20] L. Deike, E. Ghabache, G. Liger-Belair, A. K. Das, S. Zaleski, S. Popinet, and T. Séon, *Phys. Rev. Fluids* **3**, 013603 (2018).
- [21] B. W. Zeff, B. Kleber, J. Fineberg, and D. P. Lathrop, *Nature (London)* **403**, 401 (2000).
- [22] L. Duchemin, S. Popinet, C. Josserand, and S. Zaleski, *Phys. Fluids* **14**, 3000 (2002).
- [23] C. F. Brasz, C. T. Bartlett, P. L. L. Walls, E. G. Flynn, Y. Yu, and J. C. Bird, *Phys. Rev. Fluids* **3**, 074001 (2018).
- [24] S. Popinet, *J. Comput. Phys.* **190**, 572 (2003).
- [25] S. Popinet, *J. Comput. Phys.* **228**, 5838 (2009).
- [26] H. Lhuissier and E. Villermaux, *J. Fluid Mech.* **696**, 5 (2012).
- [27] P. L. L. Walls, L. Henaux, and J. C. Bird, *Phys. Rev. E* **92**, 021002 (2015).